as a marker. Specifically, administration of the luminescence substrate luciferin to these animals results in the emission of luminescence intensity that is dependent on the amount of adenosine triphosphate produced in cells, enabling us to visually and quantitatively evaluate cell viability by measuring luminescence level.

In this study, we demonstrated that graft-derived cells are capable of long-term survival and determined the role of these cells in graft acceptance. These experimental results may have an implication to the long-term survival of free bone grafts, which are commonly applied in clinical practice.

MATERIALS AND METHODS

Experimental Design

All surgical interventions and animal care were performed in accordance with Jichi Medical University Guide for Laboratory Animals. Lewis rats were purchased from Charles River Japan (Yokohama, Japan). All surgical procedures were performed under anesthesia with intraperitoneal injection of Nembutal (Abbott, Chicago, Ill.). All rats were housed in cages and allowed normal cage activity without any restrictions. All animals were euthanized by means of an anesthetic overdose injection at final evaluation. All experiments were carried out using 10-week-old male rats.

Surgical Procedure: Free Bone Transplantation and Vascularized Bone Transplantation

A vascularized tibial transplant model of the Lewis rat was established.[8] A 2.5-cm tibiofibular complex with cartilage removed from the knee joint surface on the tibial side and with a vascular pedicle of the femoral artery and vein was used as a vascularized bone graft. The vessels were anastomosed to the femoral artery and vein of a recipient rat with a 10-0 nylon suture under a microscope. The ischemic time during this procedure was approximately 30 minutes. The vascularized bone graft was implanted into a subcutaneous pocket formed in the right inguinal region, and another tibiofibular complex without a vascular pedicle collected from the other leg of the same donor rat was implanted as a free bone graft in the left inguinal region ($n = 3$). The wound was opened 14 days postoperatively, and the patency test of the anastomosed vessels was performed under a microscope. At the same time, the bone grafts were removed for histologic examination.

In Vivo Bioluminescence Imaging

Luciferase-expressing Lewis transgenic rats were used.[7] To visualize luciferase expression ex vivo and in vivo, an in vivo bioimaging system (IVIS; Xenogen, Alameda, Calif.) was used. To detect photons from luciferase-expressing cells, D-luciferin (potassium salt; Biosynth, Postfach, Switzerland) was injected into the penile vein of anesthetized rats (30 mg/kg body weight) with isoflurane (Abbott). Lucimages were taken using IVIS and quantified using the IVIS Living Image software (Xenogen) package. Data were expressed as photons per second per square centimeter per steradian.

To examine whether the living bone derived from luciferase-expressing Lewis transgenic rats emitted luminescent light, fresh bones and bones devitalized by freezing twice for 5 minutes in liquid nitrogen were tested ($n = 3$). Macroscopic images were acquired in a drop of phosphate-buffered saline. Next, iliac free bone grafts ($5 \times 5 \times 2$ mm) from luciferase-expressing Lewis transgenic rats were transplanted into the subcutaneous space of recipient wild-type Lewis rats ($n = 10$). As a control, iliac bone grafts ($5 \times 5 \times 2$ mm) were also collected from wild-type Lewis rats and transplanted into the subcutaneous pockets of recipient rats using the same procedure ($n = 4$). Post-transplantation measurement consisted of 10 sequential sessions of 1-minute measurement, so that luminescence intensity could be recorded over time.

Detection of LacZ Expression by Immunohistochemistry

LacZ-transgenic rats is derived from LEW (Rosa/LacZ-Lew) rats driven under the ROSA 26 promotor.[8] Free iliac bone transplantation ($5 \times 5 \times 2$ mm) from LacZ-transgenic rats to wild-type Lewis rats was performed ($n = 4$). Transplanted bone grafts were removed at various time points after transplantation for immunohistochemistry.

An iliac bone collected from a LacZ-transgenic rat was used as positive control, and an iliac bone collected from a wild-type Lewis rat was used as a negative control ($n = 4$). Bone tissues were fixed in 10% formalin at ambient temperature for 2 days, followed by decalcification in 10% ethylenediaminetetraacetic acid solution at ambient temperature for 14 days. Tissues were then paraffin-embedded and sliced into 5-μm sections.

LacZ expression was evaluated by immunohistochemistry using anti–β-galactosidase rabbit polyclonal antibody (1:1500; Biogenesis, Poole,

England). Sections (5 μm thick) were treated with 0.3% hydrogen peroxide and stained with the primary antibody overnight at 4°C, then with EnVision+ System/horseradish peroxidase–labeled polymer anti-rabbit antibody (1:500; DAKO, Glosstrup, Denmark) for 30 minutes at room temperature. Thereafter, specimens were stained by 3,3′-diaminobenzidine-4HCL and counterstained with Mayer's hematoxylin.

Semiquantitative Analysis of LacZ Expression in Grafted Bone by Polymerase Chain Reaction

Free iliac bone grafts (5 × 5 × 2 mm, 0.1 g) collected from LacZ-transgenic rats were transplanted into the subcutaneous space on the back of wild-type Lewis rats. The rats were then euthanized at various time points to extract DNA from bone grafts ($n = 4$). Pretransplant and posttransplant bone grafts were collected, frozen in liquid nitrogen, and crushed to prepare samples for DNA extraction. DNA extraction was performed using the DNeasy Blood & Tissue kit (Qiagen, Duesseldorf, Germany). Polymerase chain reaction was performed using Taq DNA Polymerase (Takara, Ohtsu, Japan). Specifically, polymerase chain reaction was carried out by adding primers for the internal standard glyceraldehyde-3-phosphate dehydrogenase gene (*GAPDH*) (5′-AGT GGG TGT CGC GCT GTT GAA G-3′ and 5′-GTA TCG TGG AAG GAC TCA TG-3′) and those for the *LacZ* gene (5′-ACC ACA GCC ACA GAC ATC AT-3′ and 5′-CAC CAA AGT CTC CTC CAT AG-3′)

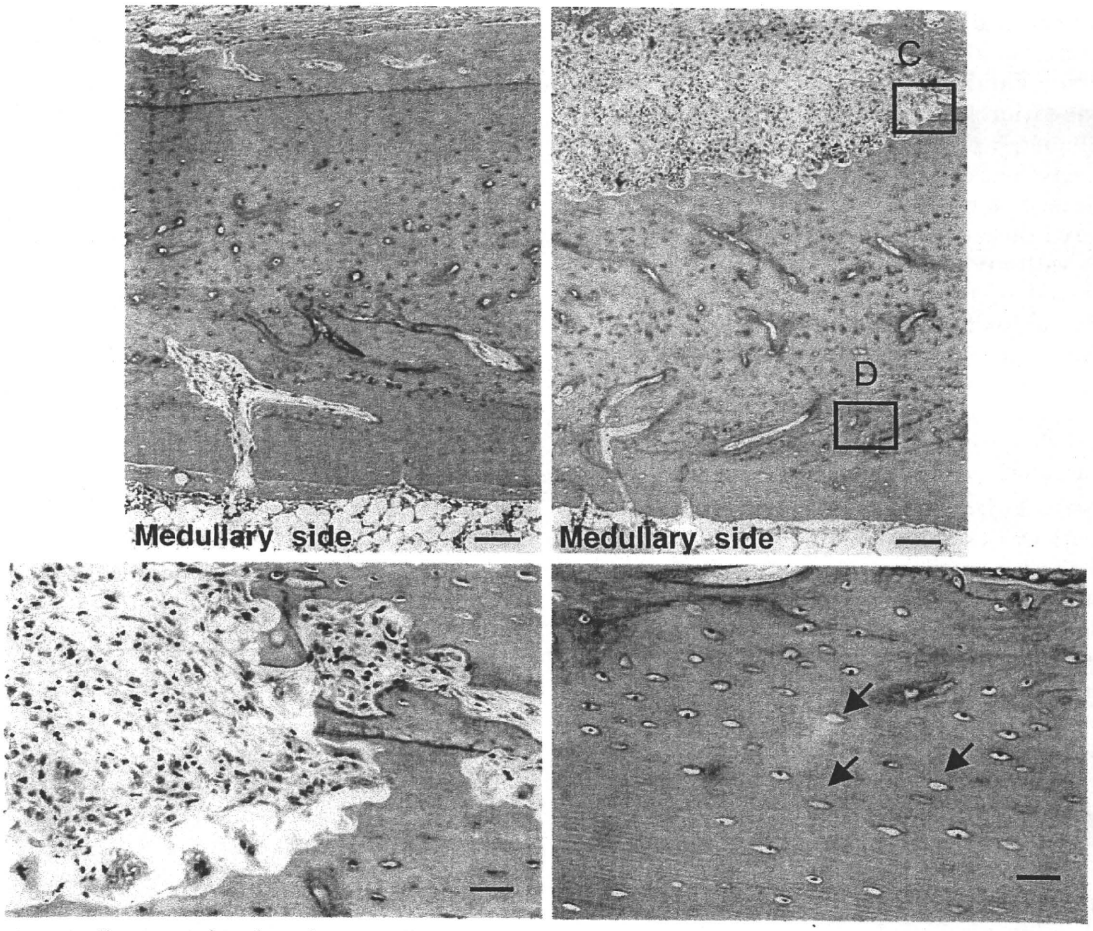

Fig. 1. Differences in histologic features of bone grafts with or without vascular reconstruction at 14 days after transplantation. (*Above, left*) Vascularized tibial bone grafts showing minimal histologic changes (hematoxylin and eosin staining, *scale bar* = 100 μm). (*Above, right*) Free tibial bone grafts showing bone resorption and replacement (hematoxylin and eosin, *scale bar* = 100 μm). (*Below, left*) Marked resorption in the edge of the bone cortex (hematoxylin and eosin, *scale bar* = 25 μm). (*Below, right*) Numerous vacuoles in bone lacunae (*arrows*) in the bone cortex (hematoxylin and eosin, *scale bar* = 50 μm).

to each sample to obtain DNA templates for quantification. Polymerase chain reaction conditions for each set of primers included an initial treatment at 95°C for 2 minutes, 55°C for 1 minute, and 72°C for 2 minutes for one cycle; and 95°C for 30 seconds, 58°C for 30 seconds, and 72°C for 1 minute for 30 cycles. Polymerase chain reaction products were analyzed using a 1% agarose gel with ethidium bromide. A standard curve was drawn from the *LacZ/GAPDH* ratio using spleen cells collected from LacZ-transgenic rats.

Analysis of Transplant Bone by Computed Tomographic Imaging

Wild-type Lewis rats transplanted with iliac bone grafts (5 × 5 × 2 mm) from luciferase-expressing Lewis transgenic rats in their back were subjected to bioluminescence imaging at 180 days after transplantation, and then euthanized (n = 10). Bone grafts were removed and subjected to computed tomographic imaging and image analysis. Computed tomographic imaging was performed using a LaTheta LCT-200 system (ALOKA, Mitaka, Japan) at a voxel size of 48 μm. Bone volume and the polar moment of inertia of area were measured with pretransplant iliac bone grafts (5 × 5 × 2 mm) used as a control (n = 4). After computed tomographic imaging, the grafts were decalcified, paraffin-embedded, and sliced into 5-μm sections for hematoxylin and eosin staining as described above.

Statistical Analysis

Data were expressed as mean ± SD, and statistical significance was determined using the Kruskal-Wallis test. A value of $p < 0.05$ was considered significant.

RESULTS

Histologic Changes Observed in the Early Phase after Transplantation

First, to examine early-phase changes in bone grafts attributable to ischemia, vascularized and free bone transplantations were performed and histologic characteristics of bone grafts were compared between the two procedures (n = 3). Vascularized tibiofibular grafts removed 14 days after transplantation showed almost intact bone morphology (Fig. 1, *above, left*). In contrast, free tibiofibular grafts showed marked resorption on the cortical bone surface (Fig. 1, *below, left*), formation of many vacuoles in bone lacunae (Fig. 1, *below, right*), and several changes suggestive of the resorption and replacement of bone grafts (Fig. 1, *above, right*). These findings suggest substantial changes in the kinetics of graft-derived cells following free bone transplantation.

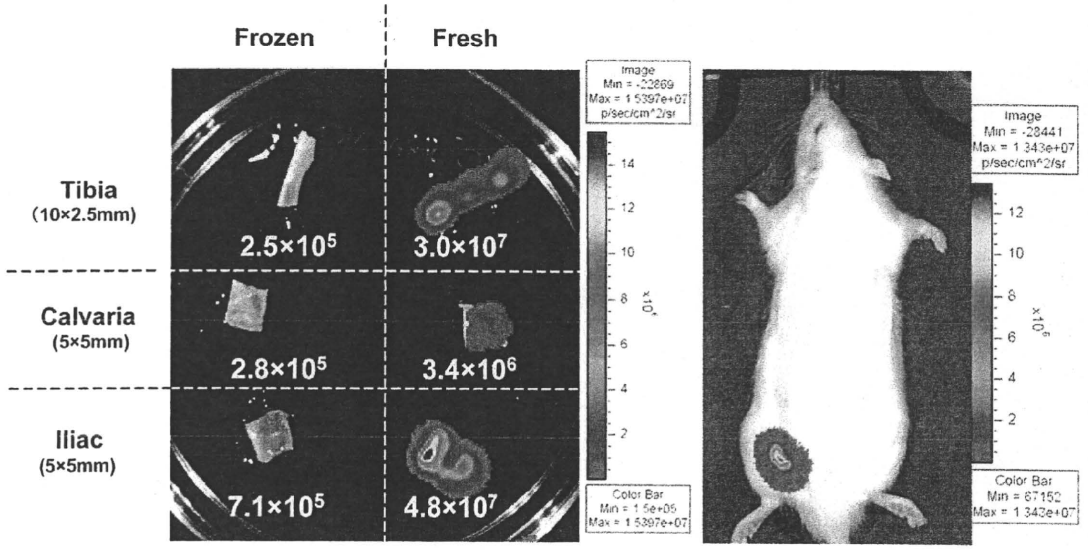

Fig. 2. Representative bioluminescence images of transplantable bones. (*Left*) Luminescence images taken after luciferin injection onto bones collected from a luciferase transgenic rat. The numbers under each bone represent the total number of photons per second. (*Right*) A luminescence image taken after luciferin injection into a wild-type rat to which a free iliac bone graft derived from a luciferase transgenic rat had been transplanted into the subcutaneous space on the back (7 days after transplantation).

Bioluminescence Imaging following Free Bone Transplantation

We determined whether we can use bone grafts from luciferase-expressing Lewis transgenic rats to examine the kinetics of free bone graft–derived cells. All fresh bones collected from luciferase-expressing Lewis transgenic rats, regardless of the type of bones, emitted a sufficient level of luminescence (mean, 2.7×10^7 photons/second; $n = 3$) (Fig. 2, *left*). Bones that had been once immersed in liquid nitrogen failed to emit luminescence (mean, 4.1×10^5 photons/second; $n = 3$). Free bone grafts from luciferase-expressing Lewis transgenic rats exhibited a substantial level of luminescence (mean, 5.1×10^7 photons/second) 7 days after transplantation (Fig. 2, *right*). These findings indicate the applicability of luciferase-expressing Lewis transgenic rat–derived bone grafts for in vivo luminescence imaging.

Changes in In Vivo Luminescent Flux Imaging after Free Bone Transplantation

Free iliac bone transplantation ($5 \times 5 \times 2$ mm) from luciferase-expressing Lewis transgenic rats to wild-type rats was performed to examine the increase and decrease in the number of graft-derived cells over time by bioluminescence imaging ($n = 10$). The time-dependent changes in the level of emitted luminescence per measurement were moderate in the early posttransplantation period (1 and 3 days after transplantation). On and after 7 days following transplantation, luminescence emission reached the maximum level immediately after the intravenous injection of the substrate and then decreased gradually (Fig. 3, *above*). The maximum luminescence emission reached its peak 14 days after transplantation and decreased thereafter until 60 days after transplantation. However, almost no decrease in lumines-

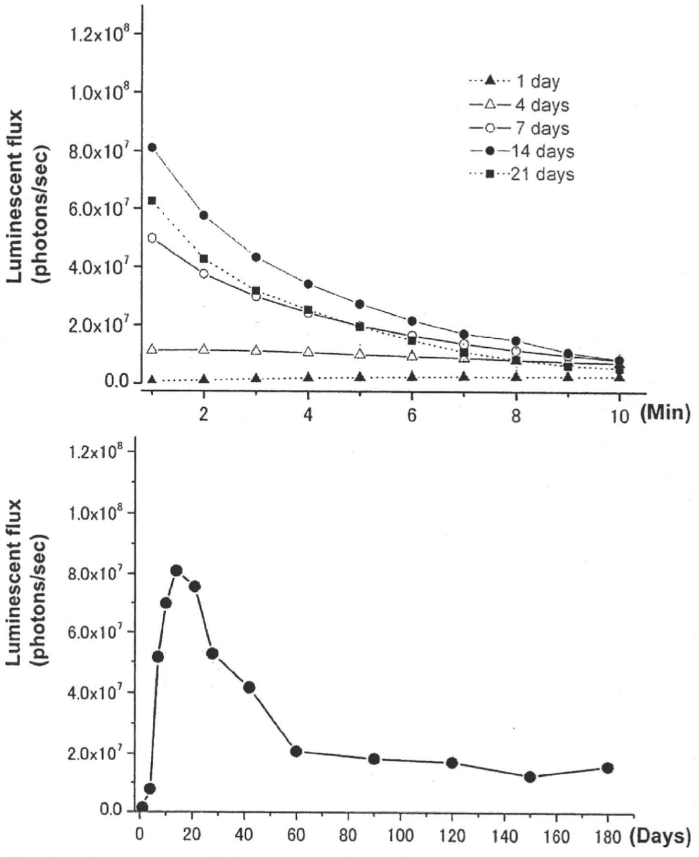

Fig. 3. Time course of photon signal in wild-type rats to which iliac bone grafts derived from luciferase transgenic rats had been transplanted into the subcutaneous space on the back. *Error bars* = SD ($n = 10$). (*Above*) Time course of luminescence emission after intravenous injection of luciferin. (*Below*) Time course of luminescence emission (in days) after bone transplantation.

cence was observed after 60 days after transplantation, with a substantial level of luminescence (mean, 1.6×10^7 photons/second) detected even at 180 days after transplantation (Fig. 3, *below*). Free iliac bone grafts ($5 \times 5 \times 2$ mm) from wild-type Lewis rats failed to emit a substantial level of luminescence even at 14 days after transplantation ($n = 4$). These findings indicate the presence of viable graft-derived cells at 180 days after transplantation.

Analysis of Free Bone Graft–Derived Cells

The kinetics of free bone graft–derived cells was examined immunohistochemically. An iliac bone collected from a LacZ-transgenic rat as a positive control showed β-galactosidase–positive osteocytes (Fig. 4, *above, left*). An iliac bone collected from a wild-type Lewis rat showed β-galactosidase–negative osteocytes (Fig. 4, *above, right*). Immunohistochemistry of LacZ-transgenic rat–derived iliac bone grafts removed 14 days after subcutaneous transplantation into wild-type Lewis rats revealed β-galactosidase–positive osteocytes and osteoblasts lining the cortical bone surface (Fig. 4, *below, left*). Tissue samples collected 28 days after transplantation also showed β-galactosidase–positive osteocytes derived from LacZ-transgenic rats (Fig. 4, *below, right*).

Changes in the number of graft-derived cells were also examined. Semiquantitative polymerase chain reaction of the *LacZ* gene was performed. A standard curve was drawn from the *LacZ/GAPDH* ratio using spleen cells derived from LacZ-transgenic rats (Fig. 5, *above* and *center*). The number of

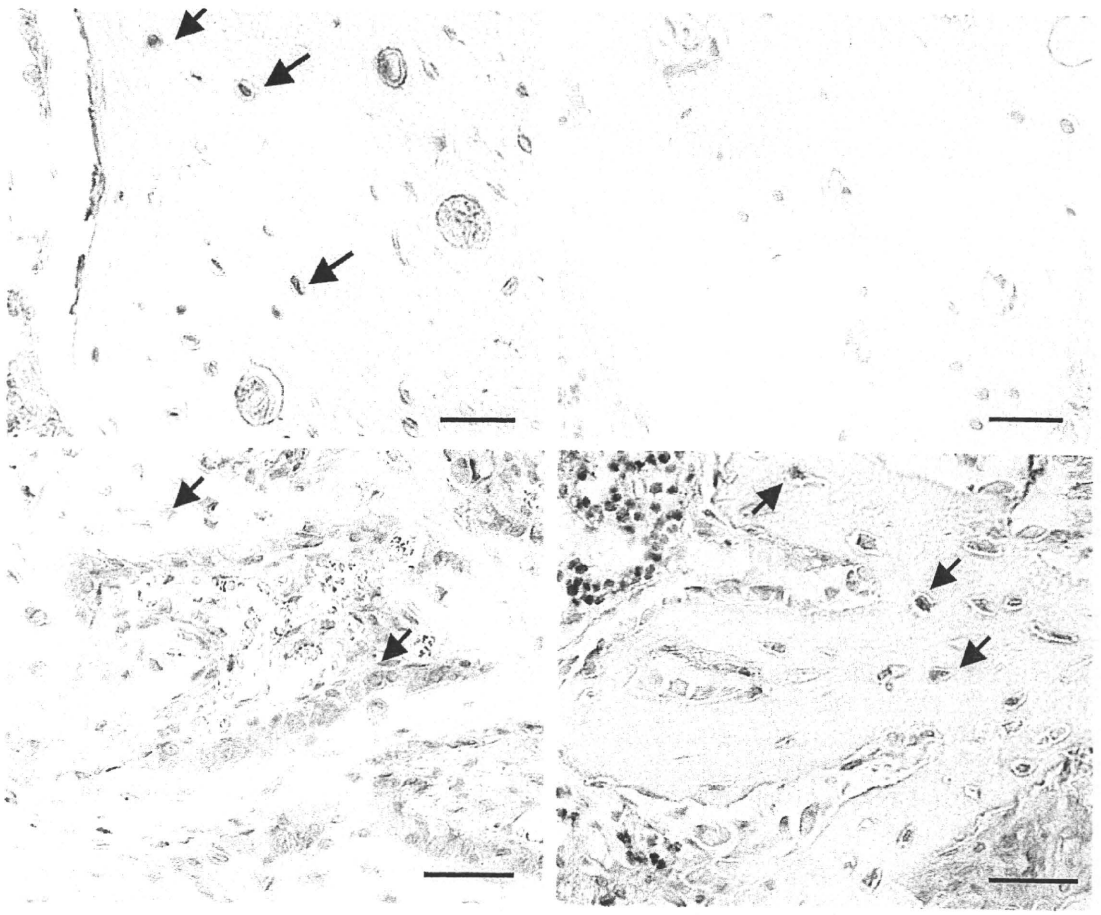

Fig. 4. Immunohistochemistry with anti-ß-galactosidase (scale bars = 50 μm). *Arrows* indicate β-galactosidase–positive cells. (*Above, left*) Iliac bone collected from a LacZ-transgenic rat used as a positive control. (*Above, right*) Iliac bone collected from a wild-type Lewis rat used as a negative control. (*Below, left*) Immunohistologic image of a LacZ-transgenic rat–derived iliac bone graft that had been transplanted into a wild-type Lewis rat for 14 days. (*Below, right*) Immunohistologic image of a LacZ-transgenic rat–derived iliac bone graft that had been transplanted into a wild-type Lewis rat for 28 days.

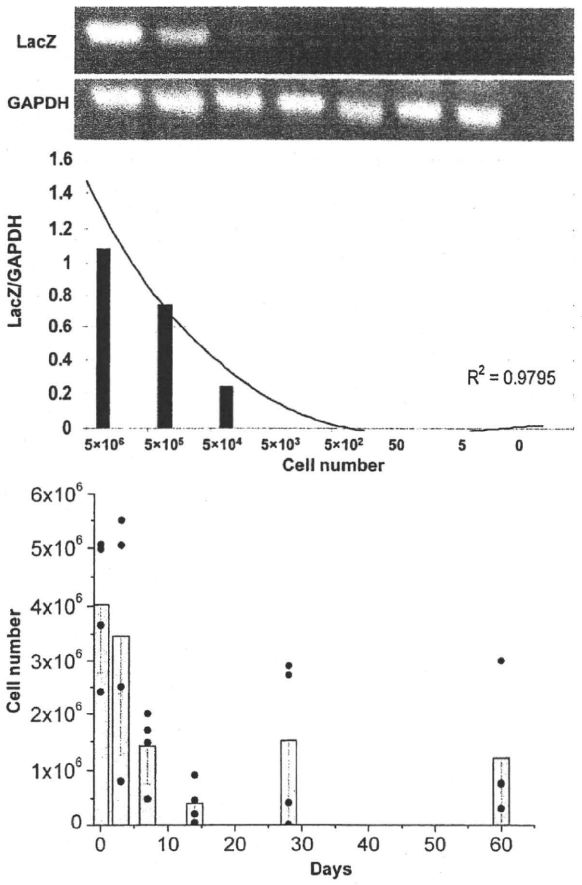

Fig. 5. (*Above*) Semiquantitative polymerase chain reaction of the *LacZ* gene to determine the number of graft-derived cells. (*Center*) A standard curve was drawn from the *LacZ/GAPDH* ratio using genome DNA extracted from spleen cells of LacZ-transgenic rats. (*Below*) Time course of the number of LacZ-positive cells in LacZ-transgenic rat–derived iliac bone grafts transplanted into wild-type Lewis rats. Columns represent means and error bars represent SD ($n = 4$).

LacZ-positive cells was determined based on the standard curve, revealing a gradual decrease in LacZ-positive donor cells after transplantation (Fig. 5, *below*). Although the number of LacZ-positive cells decreased from the pretransplant level, viable donor-derived LacZ-positive cells were observed even at 60 days after transplantation. These findings indicate the presence of viable free bone graft–derived cells at 60 days after transplantation.

Histologic and Computed Tomographic Image Analyses of Bone Grafts Removed 180 Days after Transplantation

The viability of donor-derived cells and the bone architecture following free bone transplantation were examined comparatively. Four grafts with the highest luminescence levels (mean, 2.6×10^7 photons/second) and four grafts with the lowest luminescence levels (mean, 1.0×10^7 photons/second) at 180 days after transplantation were compared by micro–computed tomographic analysis. High-luminescence free iliac bone grafts were markedly reduced in size but showed only a small number of vacuoles in bone lacunae and no inflammatory cell infiltration (Fig. 6). In contrast, low-luminescence bone grafts showed a larger number of vacuoles in bone lacunae and scattered infiltration of inflammatory cells. The three-dimensional computed tomographic image analysis of bone grafts revealed a morphologically firm bone architecture for high-luminescence grafts (Fig. 7, *left*). In contrast, marked bone resorption was observed in low-luminescence grafts (Fig. 7, *right*). The bone volume of free bone grafts was significantly reduced to 12 percent of the pretransplant iliac bone. However, the bone volume of high-luminescence grafts was still 3.05-fold larger than that of low-luminescence grafts, with a significant difference (Fig. 8, *left*). The polar moment of inertia of area, an indicator of resistance to axial torsion that is dependent on cross-sectional shape, was significantly (7.15-fold) higher in high-luminescence grafts than in low-luminescence grafts (Fig. 8, *right*). These findings suggest that grafts with more viable graft-derived cells maintain better bone architecture.

DISCUSSION

It is clinically and experimentally well known that better engraftment is achieved with fresh autologous bone grafts than with frozen preserved grafts, and by vascularized bone transplantation than by free bone transplantation.[6,9,10] Although the survival of graft-derived cells has been demonstrated by polymerase chain reaction,[11] and bone formation following transplantation of mesenchymal stem cells in a mold has been observed by bioluminescence imaging,[12] the kinetics of bone graft–derived cells has not yet been fully elucidated. In this study, we were able to determine the kinetics of graft-derived cells using bone markers expressed in almost all parts of the body in luciferase-transgenic rats.

We created a model of transplanting free bone grafts in the subcutaneous space and examined the change in the number of graft-derived cells over time by bioluminescence imaging. A slight increase in luminescence was observed following intravenous injection of luciferin in the early phase after transplantation (1 and 3 days after transplantation). In contrast, on and after 7 days

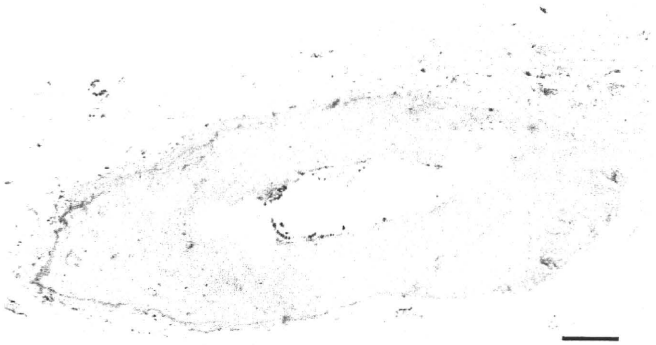

Fig. 6. The status of luciferase-transgenic rat–derived iliac bone grafts that had been transplanted in wild-type Lewis rats for 180 days was compared between subgroups based on luminescence intensity on luminescence imaging. Representative histologic image of high-luminescence bone grafts (hematoxylin and eosin staining, *scale bar* = 100 μm).

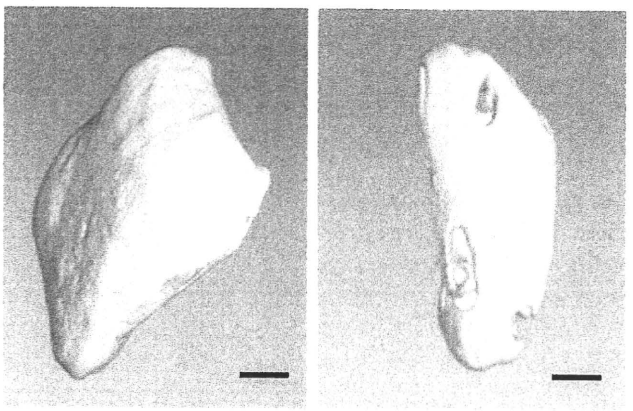

Fig. 7. (*Left*) Representative three-dimensional computed tomographic image of high-luminescence bone grafts (*scale bar* = 100 μm). (*Right*) Representative three-dimensional computed tomographic image of low-luminescence bone grafts (*scale bar* = 100 μm).

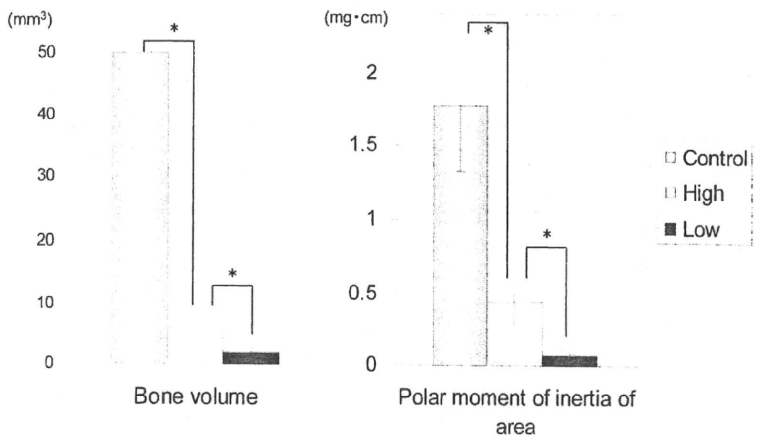

Fig. 8. (*Left*) Bone volume and (*right*) polar moment of inertia of area as indicated by the level of luminescence on luminescence imaging. Data represent mean ± SD. *$p < 0.05$; pretransplant iliac bone was used as a control.

following transplantation, luminescence reached the maximum level immediately after intravenous injection and decreased rapidly thereafter. In the presence of a sufficient amount of D-luciferin, luminescence intensity depends on the number of fluorescent photons emitted from adenosine triphosphate–producing cells incorporating luciferin. Therefore, for the precise measurement of luminescence, cells must be provided with a sufficient blood flow. This appeared not to be a major issue in other studies of bioluminescence imaging using D-luciferin,[12–14] where vascularized organs or a fixed number of cells were transplanted so that there was no major change in blood blow over time. In free tissue transplantation as performed in this study, bone grafts are not sufficiently revascularized in the early phase after transplantation and therefore luciferin is delivered to luciferase-expressing Lewis transgenic–derived bone grafts more by means of tissue diffusion than by means of blood flow. This is likely to result in an inaccurate estimation of cell number. High-intensity luminescence emission was observed immediately after intravenous injection on and after 7 days following transplantation, suggesting the establishment of blood flow to the bone graft around this period. Therefore, the time course of the maximum luminescence intensity in days after transplantation (Fig. 3, *below*) was expected to be dependent on the number of viable cells derived from luciferase-expressing Lewis transgenic rats on and after 14 days following transplantation, by which time stable blood flow is established. The trend of a gradual decrease in the number of graft-derived cells after transplantation was also observed in semiquantification analysis by polymerase chain reaction.

Identification of graft-derived cells often requires immunohistochemical examination. Immunohistochemistry of LacZ-transgenic rat–derived bone grafts retrieved 14 days after transplantation revealed positive staining for β-galactosidase in osteocytes and proliferating osteoblasts, suggesting that graft-derived cells were viable and differentiated and some of them even contributed to bone formation. Immunohistochemistry of bone grafts retrieved 28 days after transplantation also showed viable graft-derived cells as osteocytes, although the number of β-galactosidase–positive cells was reduced. These findings suggest that graft-derived cells contribute to bone reconstruction in the early phase after transplantation and can also survive for a long time as osteocytes.

There was a substantial difference in the actual architecture of bone grafts between grafts emitting high luminescence and those emitting low luminescence on bioluminescence imaging at 180 days after transplantation. High-luminescence grafts that showed no histologic evidence of inflammation were likely to continue to engraft. In contrast, low-luminescence bones that showed marked resorption on three-dimensional computed tomographic images were expected to undergo further resorption. Ectopic subcutaneous transplantation of either fresh or devitalized bone grafts has been associated with a lower rate of new bone formation than bone transplantation to replace bone defects (i.e., orthotopic transplantation).[15] Although bone regeneration is promoted by surrounding bones in orthotopic transplantation, there is less recipient-derived osteoinduction and osteoconduction in ectopic transplantation. It is thus likely that the engraftment of bone grafts depends on the number of donor-derived cells that remain viable in grafts. Considered together, the results of the study suggest that free bone graft–derived cells can survive for a long time and that the presence of a sufficient number of viable graft-derived cells is essential for graft engraftment and remodeling.

Asako Yamaguchi, M.D.
Division of Plastic Surgery
Department of Surgery
Jichi Medical University
3311-1 Yakushiji
Shimotsuke, Tochigi 329-0498, Japan
asaya-magu@umin.ac.jp

ACKNOWLEDGMENTS

This study was supported by a grant from the General Insurance Association of Japan, Tokyo, and by a research grant from the "Strategic Research Platform" Project for Private Universities: matching fund subsidy from the Ministry of Education, Culture, Sports, Science and Technology of Japan.

REFERENCES

1. Phemister DB. The fate of transplanted bone and regenerative power of its various constituents. *Surg Gynecol Obstet.* 1914;19:303–333.
2. Frame JW, Broune RM, Brady CL. Biologic basis for interpositional autogenous bone grafts to the mandible. *J Oral Maxillofac Surg.* 1982;40:407–411.
3. Deleu J, Trueta J. Vascularisation of bone grafts in the anterior chamber of the eye. *J Bone Joint Surg (Br.)* 1965;47:319–329.
4. Burwell RG. The function of bone marrow in the incorporation of a bone graft. *Clin Orthop Relat Res.* 1985;200:125–141.
5. Zhang X, Xie C, Lin AS, et al. Periosteal progenitor cell fate in segmental cortical bone graft transplantations: Implications for functional tissue engineering. *J Bone Miner Res.* 2005;20:2124–2137.

6. Kruyt MC, Delawi D, Habibovic P, Oner FC, van Blitterswijk CA, Dhert WJ. Relevance of bone graft viability in a goat transverse process model. *J Orthop Res.* 2009;27:1055–1059.
7. Hakamata Y, Murakami T, Kobayashi E. "Firefly rats" as an organ/cellular source for long-term in vivo bioluminescent imaging. *Transplantation* 2006;81:1179–1184.
8. Inoue H, Ohsawa I, Murakami T, et al. Development of new inbred transgenic strains of rats with LacZ and GFP. *Biochem Biophys Res Commun.* 2005;329:288–295.
9. Weiland AJ, Phillips TW, Randolph MA. Bone grafts: A radiologic, histologic, and biomechanical model comparing autografts, allografts, and free vascularized bone grafts. *Plast Reconstr Surg.* 1984;74:368–379.
10. Plakseychuk AY, Kim SY, Park BC, Varitimidas SE, Rubash HE, Sotereanos DG. Vascularized compared with nonvascularized fibular grafting for the treatment of osteonecrosis of the femoral head. *J Bone Joint Surg (Am.)* 2003; 85:589–596.
11. Kakinoki R, Bishop AT, Tu YK, Matsui N. Detection of the proliferated donor cells in bone grafts in rats, using a PCR for a Y-chromosome-specific gene. *J Orthop Sci.* 2002;7:252–257.
12. Olivo C, Alblas J, Verweij V, Van Zonneveld AJ, Dhert WJ, Martens AC. In vivo bioluminescence imaging study to monitor ectopic bone formation by luciferase gene marked mesenchymal stem cells. *J Orthop Res.* 2008;26:901–909.
13. Kutschka I, Chen IY, Kofidis T, et al. In vivo optical bioluminescence imaging of collagen-supported cardiac cell grafts. *J Heart Lung Transplant.* 2007;26:273–280.
14. Okada S, Ishii K, Yamane J, et al. In vivo imaging of engrafted neural stem cells: Its application in evaluating the optimal timing of transplantation for spinal cord injury. *FASEB J.* 2005;19:1839–1841.
15. Kruyt MC, Dhert WJ, Oner C, Van Blitterswijk CA, Verbout AJ, de Bruijn JD. Osteogenicity of autologous bone transplants in the goat. *Transplantation* 2004;77:504–509.

NEOPLASIA
www.neoplasia.com

Volume 13 Number 3 March 2011 pp. 206–216 206

Vascular CD39/ENTPD1 Directly Promotes Tumor Cell Growth by Scavenging Extracellular Adenosine Triphosphate[1,2]

Lili Feng[*,3], Xiaofeng Sun[*,3], Eva Csizmadia[*], Lihui Han[*], Shu Bian[*], Takashi Murakami[*], Xin Wang[*], Simon C. Robson[*,4] and Yan Wu[*,4]

[*]Department of Medicine, Transplantation Institute, Beth Israel Deaconess Medical Center, Harvard Medical School, Boston, MA, USA; [†]Division of Biomedical Sciences, Center for Molecular Medicine, Iwate Medical University, Shimotsuke, Tochigi, Japan; [‡]Department of Hematology, Provincial Hospital Affiliated to Shandong University, Jinan, PR China

Abstract

Extracellular adenosine triphosphate (ATP) is known to boost immune responses in the tumor microenvironment but might also contribute directly to cancer cell death. CD39/ENTPD1 is the dominant ectonucleotidase expressed by endothelial cells and regulatory T cells and catalyzes the sequential hydrolysis of ATP to AMP that is further degraded to adenosine by CD73/ecto-5′-nucleotidase. We have previously shown that deletion of *Cd39* results in decreased growth of transplanted tumors in mice, as a result of both defective angiogenesis and heightened innate immune responses (secondary to loss of adenosinergic immune suppression). Whether alterations in local extracellular ATP and adenosine levels as a result of CD39 bioactivity directly affect tumor growth and cytotoxicity has not been investigated to date. We show here that extracellular ATP exerts antitumor activity by directly inhibiting cell proliferation and promoting cancer cell death. ATP-induced antiproliferative effects and cell death are, in large part, mediated through $P2X_7$ receptor signaling. Tumors in *Cd39* null mice exhibit increased necrosis in association with $P2X_7$ expression. We further demonstrate that exogenous soluble NTPDase, or CD39 expression by cocultured liver sinusoidal endothelial cells, stimulates tumor cell proliferation and limits cell death triggered by extracellular ATP. Collectively, our findings indicate that local expression of CD39 directly promotes tumor cell growth by scavenging extracellular ATP. Pharmacological or targeted inhibition of CD39 enzymatic activity may find utility as an adjunct therapy in cancer management.

Neoplasia (2011) 13, 206–216

Introduction

Adenosine triphosphate (ATP) mediates multiple physiological reactions and plays a crucial role in cellular metabolism, inclusive of roles in bioenergetics [1–3]. Extracellular ATP acts on type 2 purinergic (P2) receptors to exert signaling effects. There are two P2 families: seven P2X ion channel receptors recognizing ATP ($P2X_{1\text{-}7}$) and eight P2Y G protein–coupled receptors ($P2Y_{1,\ 2,\ 4,\ 6,\ 11\text{-}14}$) that bind several nucleoside triphosphates and diphosphates [4–6]. Documented cytotoxic effects of extracellular ATP on various malignant cells have elicited attention to this signaling pathway [2,7–10]. Five P2 receptor subtypes have been considered to be involved in the antitumor actions of ATP, namely $P2X_5$, $P2X_7$, $P2Y_1$, $P2Y_2$, and $P2Y_{11}$ (exclusively in human), but precise roles for these receptors are not well defined [2,9,11].

Abbreviations: ATP, adenosine triphosphate; ADP, adenosine diphosphate; AMP, adenosine monophosphate; ENTPD1, ectonucleoside triphosphate diphosphohydrolase 1; LSEC, liver sinusoidal endothelial cell; Treg, regulatory T cells; TLC, thin-layer chromatography; wt, wild type; Luc-B16/F10, luciferase-expressing B16/F10 cells

Address all correspondence to: Yan Wu, PhD, Beth Israel Deaconess Medical Center, 330 Brookline Ave, E/CLS-614, Boston, MA 02215. E-mail: ywu@bidmc.harvard.edu

[1]This study was supported by funds from National Institutes of Health (National Heart, Lung, and Blood Institute grants PO1-HL076540 and RO1-HL094400). L. Feng was a recipient of a scholarship from the China Scholarship Council. The authors disclose no conflicts.

[2]This article refers to supplementary materials, which are designated by Table W1 and Figures W1 to W4 and are available online at www.neoplasia.com.

[3]These authors contributed equally to the work.

[4]These authors share senior coauthorship.

Received 13 September 2010; Revised 19 November 2010; Accepted 29 November 2010

 1522-8002/11/$25.00
DOI 10.1593/neo.101332

Intracellular ATP concentrations are typically of the order of 3 to 10 mM. Basal concentrations of extracellular ATP, in contrast, are considered to be around 10 nM. The latter levels are maintained by ectonucleotidases, which hydrolyze released ATP sequentially to adenosine diphosphate (ADP), adenosine monophosphate (AMP), and further to adenosine [12]. These ectoenzymes result in a 10^6-fold gradient for potential ATP efflux. Therefore, the release of a small amount of intracellular ATP could elicit a dramatic elevation of extracellular ATP concentration thereby affecting purinergic signaling [13].

Anticancer chemotherapies directly induce tumor cell death. Dying tumor cells release mediators that signal cellular damage (e.g., uric acid, nucleic acids, alum, high mobility group box 1 protein) [14,15]. These signals may be recognized by dendritic cells, which further provoke anticancer immune responses [16–18]. ATP has been recently identified as a novel danger signal emitted by dying tumor cells and is also released by immune cells. ATP is considered important for the efficient immune responses required for the successful anticancer therapies [19]. ATP can also be released from the cytosol of necrotic cells, which are always present in the center of fast-growing tumors [11], such as in transplanted melanomas [20,21].

CD39/ENTPD1 (ectonucleoside triphosphate diphosphohydrolase 1) is the dominant ectonucleotidase expressed by endothelial cells (ECs) and regulatory T cells (Treg) [22–24]. We have previously demonstrated that deletion of *Cd39* results in reduction of melanoma growth and inhibition of pulmonary metastases, associated with abrogation of angiogenesis [20]. We have also recently shown that CD39 expression on Treg inhibits NK cell–mediated antitumor activity and is permissive for hepatic metastatic tumor growth, whereas vascular CD39 boosts angiogenesis [21]. When ATP appears in the extracellular space of tumor microenvironment, it is quickly metabolized by CD39 to AMP. Therefore, in *Cd39* null mice, failure of removal of ATP released by necrotic tumor cells in the center of fast-growing tumors might cause acute increases in levels of local extracellular ATP and result in killing of adjacent tumor cells.

Given that CD39 has been implicated in promoting tumor growth and metastases through the suppression of antitumor immune responses and enhancement of angiogenesis [20,21], we further hypothesized that CD39 expression by ECs might directly protect tumor cells from high levels of extracellular ATP (from whatever source). In this study, we demonstrate that extracellular ATP directly limits tumor cell growth and that these antitumor effects could be mitigated by provision of CD39/apyrase or by the intrinsic EC expression of CD39. Targeting the expression and/or ectoenzymatic activity of CD39 in combination with other chemotherapy regimens might provide a novel approach to cancer therapy.

Materials and Methods

Mice

Eight- to twelve-week-old male *Cd39* null and *Cd73* null mice on the C57BL/6 background (have been interbred and backcrossed ×12) were used [23,25]. Age-, sex-, and strain-matched wild-type mice were purchased from Taconic (Hudson, NY). All experimental mice were kept in a temperature-controlled room with alternating 12-hour dark-light cycles. Animal experimentation protocols were reviewed and approved by the Institutional Animal Care and Use Committees of Beth Israel Deaconess Medical Center.

Tumor Cell Lines

Luciferase-expressing B16/F10 (luc-B16/F10), a genetically modified C57BL/6 mouse melanoma cell line, was established as previously described [26]. Syngeneic C57BL/6 murine MCA38 colon cancer cells were provided by Dr Nicholas P. Restifo (National Cancer Institute). All cell lines were tested for *Mycoplasma* and other infections by mouse IMPACT III PCR Profile using RADIL (Columbia, MO) and were maintained as described previously [21].

Antibodies and Reagents

Rabbit anti-$P2X_7$ antibody was purchased from Alomone Laboratories (Jerusalem, Israel) [27,28]. Mouse anti–β-actin monoclonal antibody was from Abcam (Cambridge, MA). The rabbit antibodies against cleaved caspase-3 (Asp175), cleaved caspase-9 (Asp353), caspase-3 (8G10), and caspase-9 were purchased from Cell Signaling Technology (Danvers, MA). Rat anti–mouse CD31 antibody was obtained from R&D Systems (Minneapolis, MN). The production of rabbit polyclonal anti–mouse CD39 antibody (C9F) has been described previously [29]. ^{3}H-thymidine was purchased from Perkin-Elmer (Waltham, MA). All chemicals were obtained from Sigma-Aldrich (St Louis, MO), unless otherwise stated.

Assessment of Cell Proliferation and Cell Viability

Cells (5×10^3) were seeded into 96-well plates and cultured for 24 hours. Nucleotides were then added into cultures. Sixteen hours later, cell viability was analyzed using Cell Counting Kit-8 (Dojindo Molecular Technologies, Inc, Rockville, MD) following the manufacturer's instructions. In parallel, ^{3}H-thymidine (1 μCi/well) was added into the cultures immediately after addition of nucleotides, and cell proliferation was evaluated 16 hours later using ^{3}H-TdR incorporation method as described previously [30].

In Situ *Cellular Analysis*

Cells (5×10^3) were seeded into Corning 3603 Black 96-well plates and cultured for 24 hours before being exposed to ATP. Sixteen hours later, cell growth was evaluated using the Celigo Cytometer (Cyntellect, Inc, San Diego, CA). Cells were imaged and counted using the Celigo Cell Counting application.

Liver Sinusoidal Endothelial Cell Culture

Liver sinusoidal endothelial cells (LSECs) were isolated, and cell purity was assayed using acetylated low-density lipoprotein labeled with 1,1′-dioctadecyl-3,3,3′3′-tetramethylindo-carbocyanine perchlorate (10 μg/ml) following the manufacturer's instructions (Biomedical Technologies, Inc, Stoughton, MA) as previously described [31,32]. The purity of LSECs was greater than 99%.

Cotreatment or Coculture Experiments

For experiments with apyrase or antagonist treatment, luc-B16/F10 cells were pretreated with apyrase, KN-62 (Tocris Bioscience, Ellisville, MO), MRS-2500, or suramin for 30 minutes before being exposed to treatment of ATP. For coculture experiments, LSECs were seeded together with luc-B16/F10 cells (3×10^3) at indicated ratios of cell numbers into fibronectin-coated plates and cultured in 1:1 mixtures of LSEC medium and luc-B16/F10 medium for 24 hours before being exposed to further treatments.

Immunoblot Analysis

Cultured cells were lysed in modified RIPA buffer containing 50 mM Tris-HCl (pH 7.4), 150 mM NaCl, 0.5% sodium deoxycholate, 0.1% SDS, 1% NP-40, phosphatase inhibitors (Sigma-Aldrich), and protease inhibitor cocktail tablets (Roche Applied Science, Mannheim, Germany). The measurement of protein concentrations and detailed procedures of immunoblot analysis were described previously [33].

Reverse Transcription–Polymerase Chain Reaction and Real-time Quantitative PCR

Total RNA were extracted and purified from cells using an RNeasy kit (Qiagen, Valencia, CA). Reverse transcription was conducted on 1 μg of total RNA using ABI Prism TaqMan reverse transcription reagents (Applied Biosystems, Foster City, CA). Reverse transcription–polymerase chain reaction (RT-PCR) and real-time quantitative PCR (RQ-PCR) analyses were performed as described previously [33,34]. Specific primers for RT-PCR were obtained from Invitrogen (Carlsbad, CA), and the primer sequences were shown in Table W1. Primer probe sets of $P2X_7$ and GAPDH used for RQ-PCR were purchased from Applied Biosystems.

Flow Cytometric Analysis

After treatment of luc-B16/F10 cells with ATP or together with KN-62 for the indicated periods, apoptotic cells and necrotic cells were analyzed by staining the cells with fluorescein isothiocyanate (FITC)–annexin V and propidium iodide (PI), according to the manufacturer's instructions (apoptosis kit; BD Pharmingen, San Diego, CA). Briefly, an aliquot of 10^5 cells was incubated with FITC–annexin V and PI for 15 minutes at room temperature in the dark. Cells were then immediately analyzed by LSR II (BD Biosciences). Viable cells are not stained with FITC–annexin V or PI. The necrotic cells were FITC–annexin V and PI-positive, whereas apoptotic cells were annexin V–positive and PI-negative [35,36]. FACS data were analyzed using FlowJo software (TreeStar, Inc, Ashland, OR).

Tumor Supernatant Preparation

Luc-B16/F10 cells (5×10^5) were injected (s.c.) into flanks of wild-type C57BL/6 mice as previously established [20]. On day 14, tumors were separated, weighed, excised, and washed once with complete RPMI 1640 medium. Media were collected as "prewash" media. The tumor tissues supplemented with fresh media were then passed through a 100-μm cell strainer. The filtrates were then subjected to snap-freeze (in liquid nitrogen)–thaw cycles (twice to disrupt cell membranes), followed by centrifugation at 14,000 rpm for 30 minutes at 4°C. Supernatants were collected as "tumor supernatants" and immediately added into luc-B16/F10 cell cultures.

Measurement of ATP Levels in Biologic Samples

The "prewash" media and "tumor supernatants" were subjected to a deproteinizing sample preparation kit (BioVision, Mountain View, CA) to remove the proteins, followed by assays of ATP levels using the ATP Colorimetric/Fluorometric Assay Kit (BioVision) in accordance with the manufacturer's instructions.

Hepatic Metastatic Melanoma Model

This was preformed as described previously [21]. Briefly, luc-B16/F10 cells (2×10^5) were infused into liver through portal vein of C57BL/6 mice. After 14 days, the mice were killed and examined for tumor growth in the liver.

Immunocytohistochemistry and Immunofluorescence

These procedures were performed as previously [20,21,33,37]. Luc-B16/F10 cells (1×10^3) were seeded on poly-D-lysine/laminin–coated glass coverslips (BD Biosciences) and cultured for 4 days before being exposed to treatment.

Thin-Layer Chromatography Analysis

Enzymatic activity of freshly isolated LSECs or luc-B16/F10 cells was analyzed using thin-layer chromatography (TLC), as previously described [30,34]. A total of 3×10^5 cells were analyzed.

Statistical Analysis

All data are represented as means ± SD of values (obtained from at least three independent experiments in triplicates). All histologic and immunohistochemical images are representative of at least four mice per group. All statistical analyses were performed using the 2-tailed Student's *t* test. Significance was defined as $P < .05$.

Results

Antiproliferative Functions of ATP Are Mediated through $P2X_7$ Receptor

Luc-B16/F10 cells were used for the present study. We first examined the effects of extracellular ATP at high concentrations on the proliferation of these B16 melanoma cells. As shown in Figure 1*A*, cell proliferation was inhibited by exposure (16 hours) of ATP in a concentration-dependent manner. BzATP (synthetic nonhydrolyzable and potent ATP analogue) had more potent inhibitory effects on melanoma cell proliferation (Figure 1*B*), as expected. Similar inhibitory effects of extracellular ATP on other MCA38 colon cancer cells were also observed, albeit with differential dose-response curves (Figure W1).

To investigate involvement of P2 receptor(s) in the effects on ATP-induced proliferation, we first examined mRNA expression of all P2 receptors by RT-PCR analysis using total RNA from luc-B16/F10 cells (Figure 1*C*). Luc-B16/F10 cells expressed mRNA of several P2 receptors but not $P2X_6$, $P2Y_4$, and $P2Y_{11}$.

It has been recently reported that $P2X_7$ and $P2Y_1$ might be the major P2 receptors responsible for the antimelanoma activity of ATP in human cells [38]. Next, therefore luc-B16/F10 cells were incubated with P2 antagonists including KN-62 (to $P2X_7$), MRS-2500 (to $P2Y_1$), and suramin (nonselective to P2Rs), together with ATP (2.5 mM) for 16 hours. Changes in cell proliferation were then evaluated. Coincubation of cells with KN-62 decreased the extent of ATP-induced inhibition on melanoma cell proliferation in a dose-dependent manner (60% at 1 μM and 70% at 2.5 μM) with noted cytotoxicity of 2.5 μM KN-62 alone (Figure 1*D*). MRS-2500 (Figure 1*E*), or suramin (data not shown), failed to block the inhibitory effects of ATP.

We next performed Western blot analysis using total cell lysates from luc-B16/F10 cells to examine the protein expression of $P2X_7$ in these cells. For comparison, a human embryonic kidney (HEK293) cells line, which does not express $P2X_7$ [39], was also tested as a negative control. As shown in Figure 1*F*, $P2X_7$ was expressed in luc-B16/F10 cells. Taken together, our data suggest that $P2X_7$ receptor mediates, at least in part, the antiproliferation action of ATP in B16 melanoma cells.

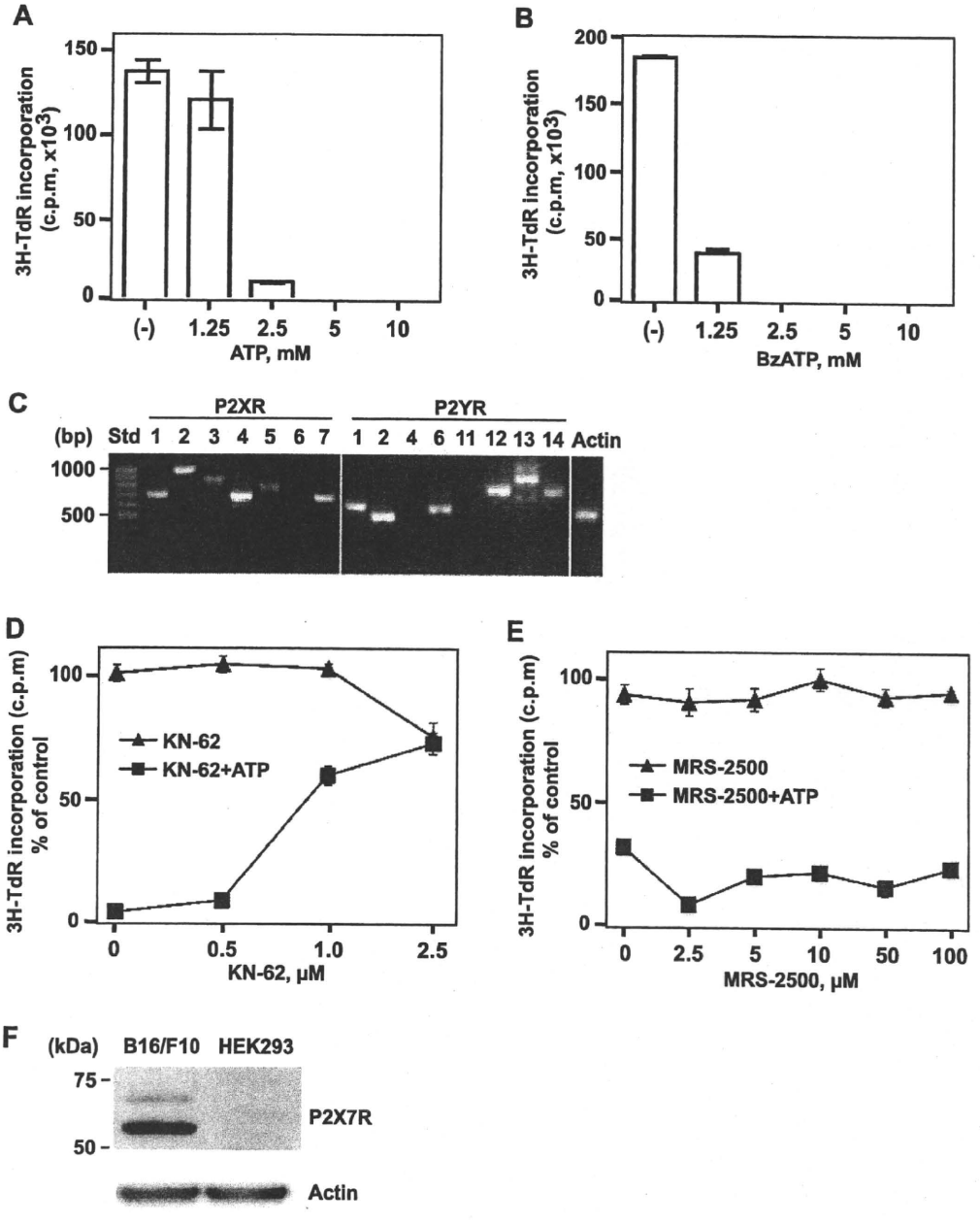

Figure 1. Antiproliferative effects of ATP on B16 melanoma cells are mediated through the $P2X_7$ receptor. High levels of extracellular ATP and BzATP inhibited melanoma cell proliferation in a dose-dependent manner. (A and B) Luc-B16/F10 cells were treated with ATP (A) or BzATP (B) at the indicated concentrations for 16 hours, and cell proliferation was determined by ^{3}H-TdR incorporation assay. Columns indicate mean of triplicate determinations; bars, SD. (C) mRNA expression of P2 receptors in luc-B16/F10 cells were determined by RT-PCR. The PCR products were visualized by agarose gel electrophoresis. The size standards (Std) are shown in the left lane. (D and E) Luc-B16/F10 cells were exposed to antagonists of P2Rs (KN-62, selective for $P2X_7$; MRS-2500, selective for $P2Y_1$), at indicated concentrations, in the presence or absence of ATP (2.5 mM) for 16 hours. Cell proliferation was assessed by ^{3}H-TdR incorporation and indicated as a percentage of untreated control cells. Points indicate mean of triplicate determinations; bars, SD. (F) Immunoblot analysis of the $P2X_7$ expression in luc-B16/F10 cells. A sample of total cell lysates (20 μg of protein) from luc-B16/F10 cells was run in parallel with a sample of HEK293 cell lysates (20 μg, negative control) and probed with $P2X_7$ antibody (top). β-Actin was used as loading control (bottom). Size standards are shown in the left lane.

ATP Promotes Tumor Cell Death through $P2X_7$ Receptor

Besides inhibition of cell proliferation, other mechanisms for antitumor function of ATP include direct induction of cell death. Dramatic decreases in cell growth caused by ATP may be also associated with cell death. We next examined the cell death after ATP exposure (Figure 2). ATP induced cytotoxicity on melanoma cells (Figure 2*A*). *In situ* cellular analysis demonstrated that melanoma cell death (Figure 2, *B-D*) with decreases in cell confluency and cell count was triggered on ATP stimulation, in a dose-dependent manner.

Similar effects were observed in MCA38 colon cancer cells albeit with different sensitivity to ATP (Figure W2 and data not shown), in keeping with data shown in Figure W1.

To precisely examine patterns of apoptosis and necrosis in the setting of ATP-induced cell death, the staining pattern of the cells were

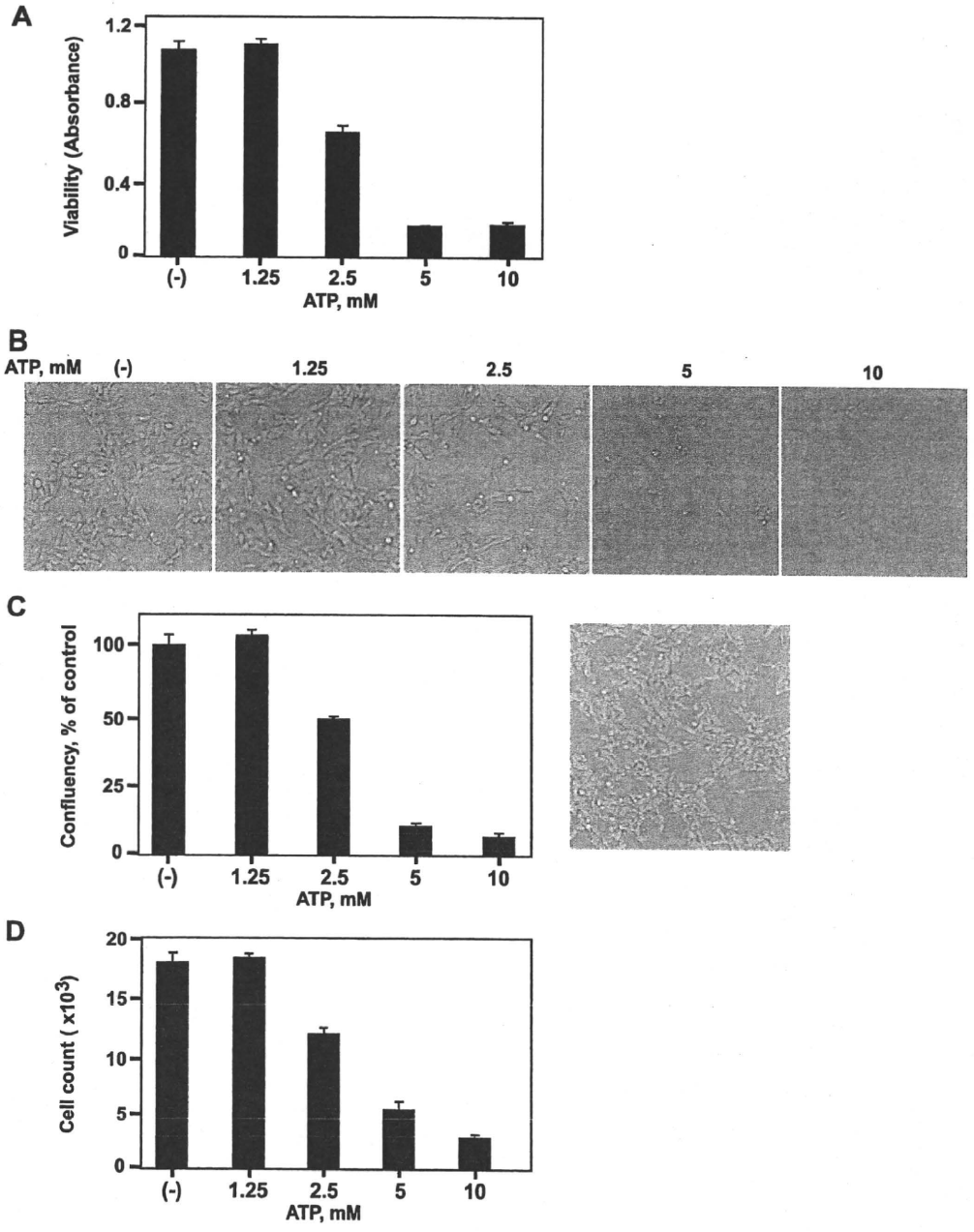

Figure 2. ATP-induced B16 melanoma cell death. Luc-B16/F10 cells were treated with ATP at the indicated concentrations for 16 hours. (A) Cell viability was measured using Cell Counting Kit-8. Cells were also imaged and counted using the Celigo Cell Counting application. (B) Representative brightfield images of live luc-B16/F10 cells. (C) Confluency of cells per well is expressed as a percentage of untreated control cells (left). Representative image of control cells with gating of confluency is shown on the right. (D) Cell count per well. Columns indicate mean of triplicate determinations; bars, SD.

analyzed with fluorescein isothiocyanate (FITC)–conjugated annexin V and PI by flow cytometry [35,36]. In this experiment, luc-B16/F10 cells treated with ATP (2.5 mM) alone or together with KN-62 (2.5 μM), or MRS-2500 (2.5 μM), or suramin (250 μM) were stained simultaneously with both FITC–annexin V and PI. Induction of both apoptosis and necrosis were observed in cells exposed to ATP in a time-dependent manner (Figure 3*A*, *top*). In addition, ATP-stimulated apoptotic/necrotic cell death could be blocked by coincubation with a $P2X_7$ antagonist, KN-62 (2.5 μM; Figure 3*A*, *bottom*), but not by coincubation of MRS-2500 or suramin (data not shown).

Next, we tested the cleavage of caspase-3 and caspase-9 as markers of apoptosis. Figure 3*B* showed that the levels of cleaved caspase-3 (Figure 3*B*, *top*), and caspase-9 (Figure 3*B*, *bottom*) increased over time after exposure to ATP. These observations were further confirmed by Western blot analysis using anti–cleaved caspase-3 and caspase-9 antibodies (Figure 3*C*, *left*). Furthermore, coincubation of cells with KN-62 (2.5 μM) blocked ATP-induced cleavage of caspase-3 and caspase-9 (Figure 3*C*, *right*).

Quantitative real-time PCR revealed that treatment with ATP (2.5 mM) for 16 hours significantly increased the mRNA expression level of $P2X_7$, whereas cotreatment with KN-62 (2.5 μM) abrogated the increase in $P2X_7$ expression (Figure 3*D*). These findings indicate that ATP-induced cell death in B16 melanoma cells is associated with both apoptosis and necrosis and is at least partly mediated through the $P2X_7$ receptor.

Apyrase (Soluble NTPDase) or Vascular Cell CD39 Expressed by LSECs Abrogates/Reverses Antitumor Activity of ATP

Next, we sought to determine whether scavenging of extracellular ATP by apyrase, a soluble form of NTPDase with ATPase and ADPase activity at a 1:1 ratio, could rescue ATP-stimulated growth inhibition of tumor cells. Figure 4*A* showed that tumor cell growth inhibition triggered by ATP (2.5 mM) was completely abrogated by coincubation of cells with apyrase (10 U/ml). The rescue of tumor cells by apyrase was dose dependent.

CD39 and CD73 are the major ectonucleotidases expressed by LSECs. Next, LSECs were purified from wt, *Cd39* null, or *Cd73* null livers and were cocultured with luc-B16/F10 cells for 24 hours, at various ratios of cell numbers, before being exposed to ATP (2.5 mM) for 16 hours.

Successful isolation of healthy LSECs was verified by uptake of DiI-labeled Ac-LDL and FACS analysis for endothelium makers (including CD31, CD34, and Flk-1) (data not shown), as established previously [31,32].

As shown in Figure 4*B*, wt LSECs attenuated the inhibitory effects of ATP on tumor cell growth, whereas *Cd39* null LSECs did not retain this capacity. Interestingly, growth inhibition by ATP was reversed by *Cd73* null LSECs to a greater extent, when compared with wt LSECs (Figure 4*B*). The rescue observed with wt and *Cd73* null LSECs was dose dependent.

We also noted that extracellular ATP inhibited growth of LSECs (Figure W3 for wt cells and data not shown for null cells).

To further investigate the mechanisms underlying the observations in Figure 4*B*, purine metabolism by ectonucleotidase activity of freshly isolated LSECs was examined by TLC analysis using ADP-C^{14} as substrate. ADP was first hydrolyzed to AMP and then to adenosine by wt LSECs. Adenosine was further degraded to hypoxanthine by wt LSECs (Figure 4*C*). *Cd73* null LSECs could only generate AMP but not adenosine (Figure 4*C*). *Cd39* null LSECs and luc-B16/F10 cells had minimal nonspecific ectonucleotidase activity, in contrast to wt LSECs (Figure 4*C*). These findings clearly explain how wt, *Cd73* null, and *Cd39* null LSECs exhibit differential salvage abilities on ATP-induced growth inhibition as observed in Figure 4*B*.

Defective Angiogenesis Is Associated with Heightened Tumor Necrosis and Increased $P2X_7$ Expression in Cd39 Null Tumor-Bearing Mice

We next determined whether injured tumor cells could release endogenous mediators that directly result in cellular damage of contiguous/adjacent tumor cells. Luc-B16/F10 cells were injected (s.c.) into flanks of wild type C57BL/6 mice for 14 days, tumors were excised, and tumor supernatants were prepared (see Materials and Methods), these were then added to luc-B16/F10 cell cultures. In Figure 5*A*, we show that melanoma cell proliferation was inhibited by the addition of tumor supernatants in a concentration-dependent manner. Dramatic increases in ATP levels were also noted in these tumor supernatants compared with the prewash media (Figure W4). However, coincubation with apyrase alone failed to rescue the growth inhibitory effects triggered by these crude tumor supernatants (data not shown) as previously noted with exogenous ATP (Figure 4*A*). These data suggest that other cytotoxic constituents besides nucleotides contribute to the tumor killing activity of supernatants.

We have recently demonstrated the effect of *Cd39* deletion on melanoma growth *in vivo* using a murine model of hepatic metastases of B16/F10 melanoma [21]. We noted that immune cell as well as vascular CD39 expression promote tumor growth, whereas pharmacological inhibition of CD39 enzymatic activity (in contrast) abrogates tumor growth [21].

We stained these liver tumor sections using anti-CD31 (a marker for endothelium) and anti-CD39 antibodies. We observed that CD39 was expressed on tumor-associated endothelial cells (ECs) in wt livers. In contrast, in *Cd39* null tumor-bearing livers, lack of CD39 expression (suggesting decreased ATP scavenging in the tumor microenvironment) was associated with defective angiogenesis and larger areas of necrosis within the centers of tumors (Figure 5*B*). Immunofluorescent staining on tumor sections further showed that protein expression of $P2X_7$ was increased on melanoma cells in *Cd39* null tumor-bearing livers compared with wt livers (Figure 5*C*).

Discussion

The present study clearly demonstrates that tumor-derived mediators, inclusive of ATP, directly exert growth inhibitory effects on tumor cells. The $P2X_7$ receptor is functionally expressed in B16/F10 melanoma cells and is responsible, at least in part, for such ATP-induced growth inhibition and cell death. Importantly, coculture of tumor cells with LSECs demonstrates that expression of ecto-enzyme CD39 by endothelial cells counteracts tumoricidal actions stimulated by extracellular ATP. Collectively, in light of ATP-induced tumor suppression, our results indicate novel purinergic mechanisms implicated in tumor biology: 1) danger signals (including ATP) released by necrotic tumor cells result in subsequent death of neighboring tumor cells and 2) CD39 expressed on ECs promotes tumor cell growth by scavenging extracellular ATP in the tumor microenvironment.

Different P2 receptor subtypes have been shown to modulate different cellular functions such as proliferation, differentiation, and apoptosis. $P2Y_1$ and $P2X_7$ receptors are expressed in human melanoma cells *in situ* and mediate apoptotic and necrotic actions of ATP [38].

The antitumor actions of these receptors contain three processes: inhibition of cell proliferation, promotion of cell differentiation (resulting in inhibition of cell proliferation), and cell death [2]. Here, we show that antitumor activity of ATP is largely due to the combination of inhibition of cell proliferation and induction of cell death. These two processes are both mediated largely through the expression of $P2X_7$.

When ATP appears in the extracellular space of tumor microenvironment, this mediator is rapidly hydrolyzed by ectonucleotidases to ADP, AMP, and, finally, adenosine [12]. Most studies to date

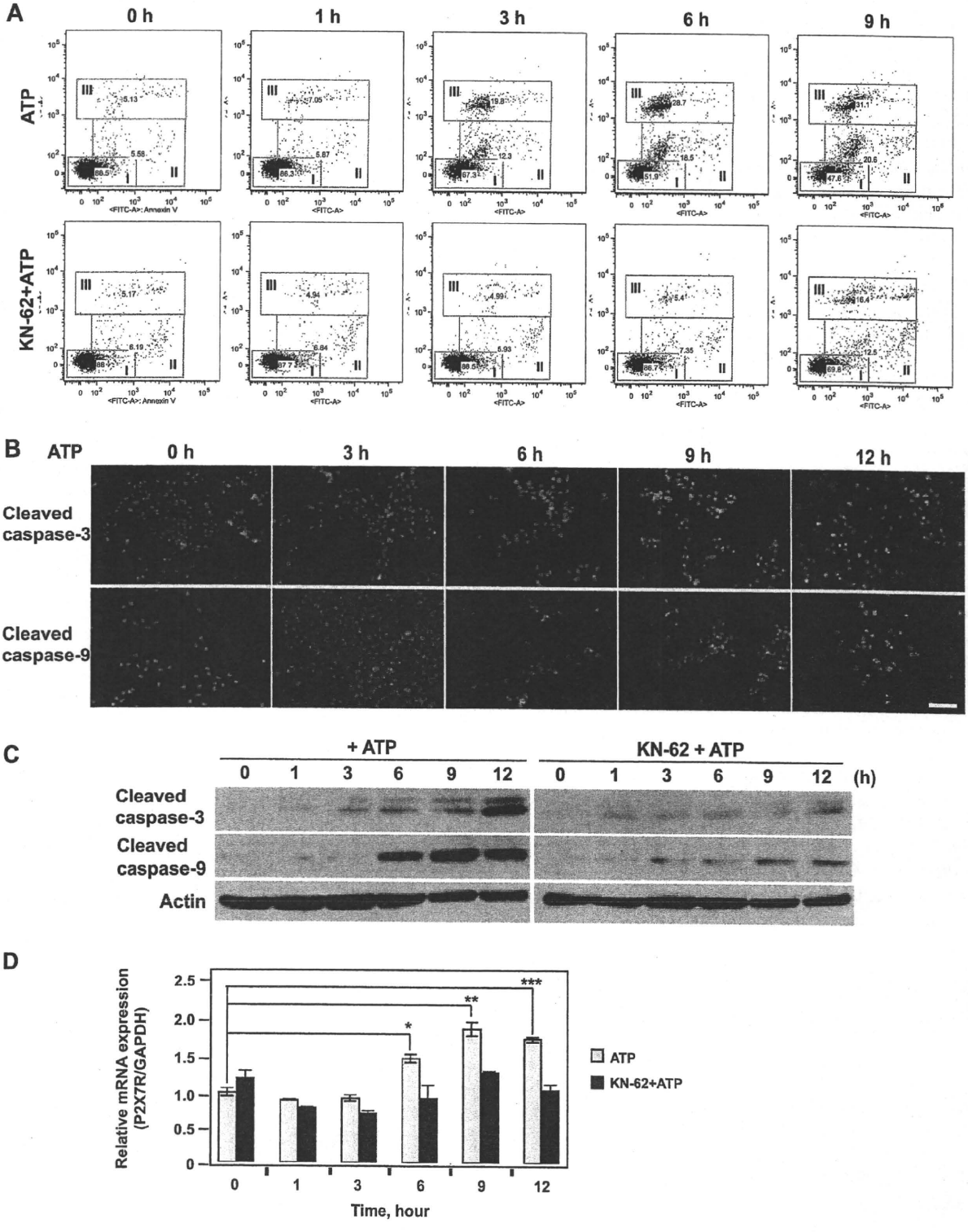

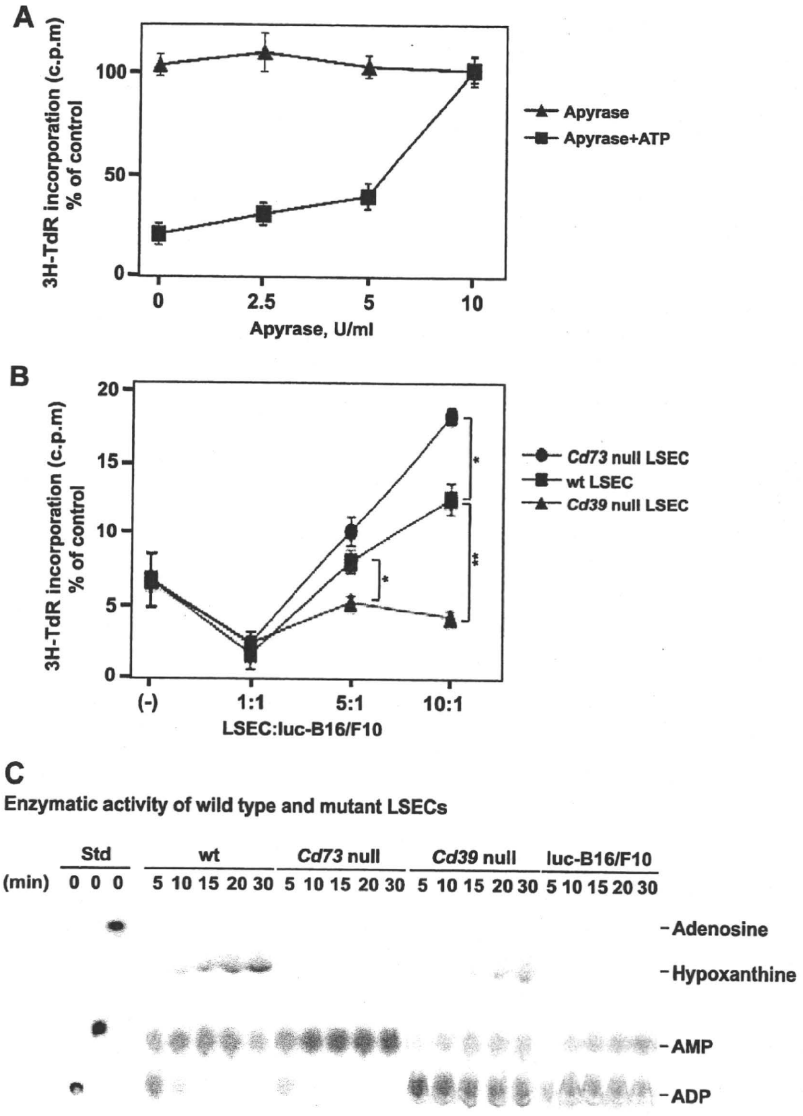

Figure 4. Apyrase (soluble NTPDase) or CD39 expression on LSECs abrogates the inhibitory effects of ATP on B16 melanoma cell growth. (A) Inhibitory effects of ATP are alleviated by addition of apyrase. Luc-B16/F10 cells were treated with apyrase at indicated concentrations for 30 minutes and then exposed to ATP (2.5 mM). Sixteen hours later, cell proliferation was analyzed by ^{3}H-TdR incorporation assay and expressed as a percentage of untreated control cells. Points indicate mean of triplicate determinations; bars, SD. (B) LSECs were isolated from C57BL/6 wild type (wt), *Cd39* null, and *Cd73* null mice and were cocultured with Luc-B16/F10 cells (3×10^5) at the indicated ratios of cell numbers for 24 hours before being exposed to ATP (2.5 mM). Cell proliferation was assayed and expressed as a percentage of untreated control cells. Points indicate mean of triplicate determinations; bars, SD. $^{*}P < .05$, $^{**}P = .002$. (C) Freshly purified LSECs or luc-B16/F10 cells (3×10^5 cells per cell type) were subjected to TLC analysis for assessment of NTPDase activity. [C^{14}]ADP, [C^{14}]AMP, and [C^{14}]ADO incubated in PBS served as standards.

Figure 3. ATP-induced apoptosis/necrosis of B16 melanoma cells is mediated through $P2X_7$ receptor. Time course of ATP-induced cell death in luc-B16/F10 cells is shown. The cells were exposed to 2.5 mM of ATP or in combination with KN-62 (2.5 μM) for the indicated periods. (A) Time course of ATP-induced apoptosis and necrosis of luc-B16/F10 cells. FITC–Annexin V/PI staining of luc-B16/F10 cells was assessed by flow cytometry at indicated times. The gates are defined as follows: I (lower left), viable; II (middle), apoptotic; and III (upper), necrotic. (B) Cells were fixed and stained with anti–cleaved caspase-3 or caspase-9 antibodies. Cleaved caspase-3 and caspase-9 were visualized by fluorescent microscopy. Representative images for each time point. Scale bar, 100 μm. The cleavage of caspase-3 and caspase-9 (red) were elevated in the cytoplasm as well as in the nuclei (blue, Hoechst dye 33258) in a time-dependent manner. (C) Cells were harvested, lysed, and used for immunoblot analysis of cleavage of caspase-3 (top) and caspase-9 (middle). Twenty micrograms of protein was loaded per lane, and gel loading was normalized by β-actin (bottom). (D) RQ-PCR analysis of $P2X_7$ mRNA expression in luc-B16/F10 cells after treatment. Columns indicate mean of triplicate determinations; bars, SD. $^{*}P = .01$, $^{**}P = .001$, $^{***}P = .002$.

have focused on the alterations of purinergic receptors in tumors, whereas ectonucleotidases are much less investigated. Purinergic signaling can be modulated by modifying the expression and/or activity of these ectoenzymes in addition to changes in P2 receptor levels [11,40].

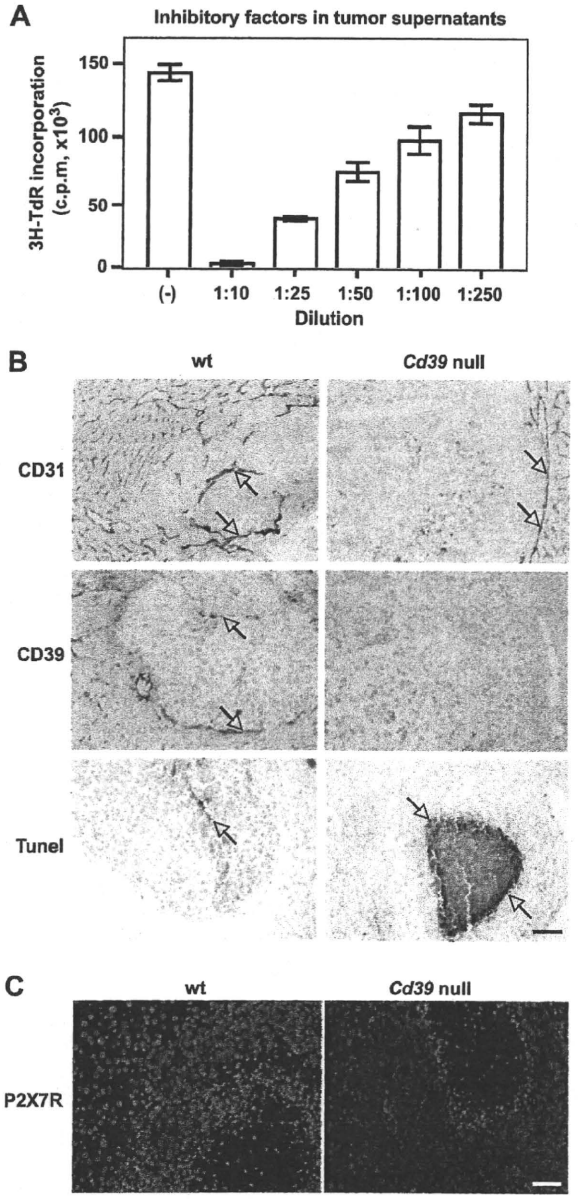

Figure 5. Metastatic melanoma growth in *Cd39* null mice. (A) Dose-dependent inhibitory effects of tumor supernatants (16 hours of treatment) on luc-B16/F10 melanoma cell proliferation. (B) Representative immunohistochemical staining on tumor tissue sections obtained from melanoma metastasized to mouse livers using anti-CD31 (a marker for endothelium) and anti-CD39 antibodies and TUNEL staining (TdT) for apoptosis. (C) $P2X_7$ expression on tumor tissues. Representative fluorescence immunohistochemical staining using anti-$P2X_7$ antibody: Hoechst dye 33258 staining nuclei in blue and $P2X_7$ in red. Columns indicate mean of triplicate determinations; bars, SD. Scale bar, 100 μm.

This study shows for the first time that deletion of *Cd39* on ECs enhances antitumor activity of ATP, whereas deletion of *Cd73* on ECs has different effects. These data suggest a feasible approach to augment anticancer therapy by modulating expression and/or enzymatic activity of NTPDase-type ectonucleotidases. This approach might be easier to achieve and more efficacious than to independently target several purinergic receptors.

CD39 is also expressed by immune cells inclusive of Treg ($CD4^+$ $Foxp3^+$) and memory cells ($CD4^+CD44^+CD62L^-Foxp3^-$) [21,41]. These cells often infiltrate into solid tumors [21]. Whether these $CD39^+$ infiltrating immune cell populations also contribute to degradation of cytotoxic ATP in the tumor microenvironment and thereby independently promote tumor growth remains unclear.

Exposure of ECs to elevated levels of ATP has been shown to promote apoptosis *in vitro* [42]. We have previously demonstrated that inhibition of tumor growth in *Cd39* null mice is associated with defects of tumor angiogenesis [20,21]. Moreover, in this study, we show that ATP also exhibits direct growth inhibitory effects on LSECs (Figure W3 and data not shown) that further compromises cell-associated NTPDase activity. Therefore, the reduction of tumor size and volume in *Cd39* null tumor-bearing mice might result from dual actions of ATP on tumor cells as well as on ECs.

The phosphohydrolysis of ATP to adenosine has a complex modulatory effect on tumor cell proliferation and growth [43–45]. Adenosine ultimately derived from ATP may be responsible for some of the observed effects as this nucleoside has been shown to affect tumor growth in a cell-specific manner determined by concentrations and kinetics of exposure [43–45] (and unpublished observations in our laboratory). Tumor cell expressions of A2A and A2B have been shown to be proapoptotic and have antitumor activity [44,45]. The actions of A3 are contradictory. Most studies have demonstrated that A3 agonists induce apoptosis and tumor growth inhibition [45–48], whereas others show that A3 stimulation blocks A2A-induced cell death and ensures cell survival [43].

Therefore, the ambient vascular nucleotide/nucleoside milieu as regulated by ectonucleotidases and ectonucleotidases dictates the efficacy of antitumor activity of ATP *in vivo*. In this study, the differential salvage abilities on ATP-triggered tumor cell growth inhibition and NTPDase activity exhibited by wt, *Cd73* null, and *Cd39* null LSECs (Figure 4, *B* and *C*) are indicative of the participation of ATP-derived adenosine in the antitumor function of ATP.

Dzhandzhugazyan et al. [49] have shown that CD39 is the major ectonucleotidase in human melanocytes and melanoma cell lines and CD39 is overexpressed in differentiated human melanomas. It has been recently reported that CD73 is expressed on various tumor cells (e.g., ID8 ovarian cancer cells) and participates in adenosine generation, thereby suppressing antitumor immune responses [50], but potentially also affecting cancer cell apoptosis.

We therefore also examined the expression of CD39 and CD73 on tumor cells used for this study. Neither CD39 nor CD73 expression was observed on cultured B16/F10 or MCA38 cells as well as on malignant cells in metastatic tumors in the livers and lungs at any progression stage after tumor challenge [20,21] (data not shown).

Lastly, we have also shown that ATP exhibits cytotoxic effects on MCA38 colon cancer cells as well, suggesting general feature of antitumor capability of ATP (Figures W1 and W2; data not shown).

In summary, we postulate an intriguing mechanism by which extracellular ATP released by dying tumor cells accumulates to high concentrations that not only function as danger signals to the im-

mune system but also can directly kill adjacent tumor cells. Our data showing that the antitumor activities of ATP are dose-dependent and can be amplified by inhibition of ectonucleotidase, such as CD39, open new avenues for investigation in cancer management.

Acknowledgments

The authors sincerely thank Nicholas P. Restifo (National Cancer Institute) for the MCA38 cells.

References

[1] Burnstock G and Knight GE (2004). Cellular distribution and functions of P2 receptor subtypes in different systems. *Int Rev Cytol* **240**, 31–304.

[2] Shabbir M and Burnstock G (2009). Purinergic receptor–mediated effects of adenosine 5′-triphosphate in urological malignant diseases. *Int J Urol* **16**, 143–150.

[3] Burnstock G (2006). Purinergic P2 receptors as targets for novel analgesics. *Pharmacol Ther* **110**, 433–454.

[4] Burnstock G and Kennedy C (1985). Is there a basis for distinguishing two types of P2-purinoceptor? *Gen Pharmacol* **16**, 433–440.

[5] Burnstock G (2006). Purinergic signalling—an overview. *Novartis Found Symp* **276**, 26–48; discussion 48–57, 275–281.

[6] Burnstock G (2007). Purine and pyrimidine receptors. *Cell Mol Life Sci* **64**, 1471–1483.

[7] Rapaport E (1983). Treatment of human tumor cells with ADP or ATP yields arrest of growth in the S phase of the cell cycle. *J Cell Physiol* **114**, 279–283.

[8] Rapaport E (1988). Experimental cancer therapy in mice by adenine nucleotides. *Eur J Cancer Clin Oncol* **24**, 1491–1497.

[9] White N and Burnstock G (2006). P2 receptors and cancer. *Trends Pharmacol Sci* **27**, 211–217.

[10] Shabbir M, Thompson C, Jarmulowiczc M, Mikhailidis D, and Burnstock G (2008). Effect of extracellular ATP on the growth of hormone-refractory prostate cancer *in vivo*. *BJU Int* **102**, 108–112.

[11] Deli T and Csernoch L (2008). Extracellular ATP and cancer: an overview with special reference to P2 purinergic receptors. *Pathol Oncol Res* **14**, 219–231.

[12] Zimmermann H (2000). Extracellular metabolism of ATP and other nucleotides. *Naunyn Schmiedebergs Arch Pharmacol* **362**, 299–309.

[13] Trautmann A (2009). Extracellular ATP in the immune system: more than just a "danger signal". *Sci Signal* **2**, pe6.

[14] Behrens MD, Wagner WM, Krco CJ, Erskine CL, Kalli KR, Krempski J, Gad EA, Disis ML, and Knutson KL (2008). The endogenous danger signal, crystalline uric acid, signals for enhanced antibody immunity. *Blood* **111**, 1472–1479.

[15] Apetoh L, Ghiringhelli F, Tesniere A, Obeid M, Ortiz C, Criollo A, Mignot G, Maiuri MC, Ullrich E, Saulnier P, et al. (2007). Toll-like receptor 4–dependent contribution of the immune system to anticancer chemotherapy and radiotherapy. *Nat Med* **13**, 1050–1059.

[16] Mariathasan S, Weiss DS, Newton K, McBride J, O'Rourke K, Roose-Girma M, Lee WP, Weinrauch Y, Monack DM, and Dixit VM (2006). Cryopyrin activates the inflammasome in response to toxins and ATP. *Nature* **440**, 228–232.

[17] Martins I, Tesniere A, Kepp O, Michaud M, Schlemmer F, Senovilla L, Seror C, Metivier D, Perfettini JL, Zitvogel L, et al. (2009). Chemotherapy induces ATP release from tumor cells. *Cell Cycle* **8**, 3723–3728.

[18] Aymeric L, Apetoh L, Ghiringhelli F, Tesniere A, Martins I, Kroemer G, Smyth MJ, and Zitvogel L (2010). Tumor cell death and ATP release prime dendritic cells and efficient anticancer immunity. *Cancer Res* **70**, 855–858.

[19] Ghiringhelli F, Apetoh L, Tesniere A, Aymeric L, Ma Y, Ortiz C, Vermaelen K, Panaretakis T, Mignot G, Ullrich E, et al. (2009). Activation of the NLRP3 inflammasome in dendritic cells induces IL-1β–dependent adaptive immunity against tumors. *Nat Med* **15**, 1170–1178.

[20] Jackson SW, Hoshi T, Wu Y, Sun X, Enjyoji K, Cszimadia E, Sundberg C, and Robson SC (2007). Disordered purinergic signaling inhibits pathological angiogenesis in cd39/Entpd1-null mice. *Am J Pathol* **171**, 1395–1404.

[21] Sun X, Wu Y, Gao W, Enjyoji K, Csizmadia E, Muller CE, Murakami T, and Robson SC (2010). CD39/ENTPD1 expression by $CD4^+Foxp3^+$ regulatory T cells promotes hepatic metastatic tumor growth in mice. *Gastroenterology* **139**(3), 1030–1040.

[22] Plesner L (1995). Ecto-ATPases: identities and functions. *Int Rev Cytol* **158**, 141–214.

[23] Enjyoji K, Sevigny J, Lin Y, Frenette PS, Christie PD, Esch JS II, Imai M, Edelberg JM, Rayburn H, Lech M, et al. (1999). Targeted disruption of cd39/ATP diphosphohydrolase results in disordered hemostasis and thromboregulation. *Nat Med* **5**, 1010–1017.

[24] Robson SC, Wu Y, Sun X, Knosalla C, Dwyer K, and Enjyoji K (2005). Ectonucleotidases of CD39 family modulate vascular inflammation and thrombosis in transplantation. *Semin Thromb Hemost* **31**, 217–233.

[25] Mills JH, Thompson LF, Mueller C, Waickman AT, Jalkanen S, Niemela J, Airas L, and Bynoe MS (2008). CD73 is required for efficient entry of lymphocytes into the central nervous system during experimental autoimmune encephalomyelitis. *Proc Natl Acad Sci USA* **105**, 9325–9330.

[26] Sato A, Ohtsuki M, Hata M, Kobayashi E, and Murakami T (2006). Antitumor activity of IFN-λ in murine tumor models. *J Immunol* **176**, 7686–7694.

[27] Jun DJ, Kim J, Jung SY, Song R, Noh JH, Park YS, Ryu SH, Kim JH, Kong YY, Chung JM, et al. (2007). Extracellular ATP mediates necrotic cell swelling in SN4741 dopaminergic neurons through $P2X_7$ receptors. *J Biol Chem* **282**, 37350–37358.

[28] Kunzli BM, Nuhn P, Enjyoji K, Banz Y, Smith RN, Csizmadia E, Schuppan D, Berberat PO, Friess H, and Robson SC (2008). Disordered pancreatic inflammatory responses and inhibition of fibrosis in CD39-null mice. *Gastroenterology* **134**, 292–305.

[29] Kaczmarek E, Koziak K, Sevigny J, Siegel JB, Anrather J, Beaudoin AR, Bach FH, and Robson SC (1996). Identification and characterization of CD39/vascular ATP diphosphohydrolase. *J Biol Chem* **271**, 33116–33122.

[30] Deaglio S, Dwyer KM, Gao W, Friedman D, Usheva A, Erat A, Chen JF, Enjyoji K, Linden J, Oukka M, et al. (2007). Adenosine generation catalyzed by CD39 and CD73 expressed on regulatory T cells mediates immune suppression. *J Exp Med* **204**, 1257–1265.

[31] LeCouter J, Moritz DR, Li B, Phillips GL, Liang XH, Gerber HP, Hillan KJ, and Ferrara N (2003). Angiogenesis-independent endothelial protection of liver: role of VEGFR-1. *Science* **299**, 890–893.

[32] Beldi G, Wu Y, Sun X, Imai M, Enjyoji K, Csizmadia E, Candinas D, Erb L, and Robson SC (2008). Regulated catalysis of extracellular nucleotides by vascular CD39/ENTPD1 is required for liver regeneration. *Gastroenterology* **135**, 1751–1760.

[33] Wu Y, Sun X, Kaczmarek E, Dwyer KM, Bianchi E, Usheva A, and Robson SC (2006). RanBPM associates with CD39 and modulates ecto-nucleotidase activity. *Biochem J* **396**, 23–30.

[34] Beldi G, Wu Y, Banz Y, Nowak M, Miller L, Enjyoji K, Haschemi A, Yegutkin GG, Candinas D, Exley M, et al. (2008). Natural killer T cell dysfunction in CD39-null mice protects against concanavalin A–induced hepatitis. *Hepatology* **48**, 841–852.

[35] Koopman G, Reutelingsperger CP, Kuijten GA, Keehnen RM, Pals ST, and van Oers MH (1994). Annexin V for flow cytometric detection of phosphatidylserine expression on B cells undergoing apoptosis. *Blood* **84**, 1415–1420.

[36] Vermes I, Haanen C, Steffens-Nakken H, and Reutelingsperger C (1995). A novel assay for apoptosis. Flow cytometric detection of phosphatidylserine expression on early apoptotic cells using fluorescein labelled annexin V. *J Immunol Methods* **184**, 39–51.

[37] Goepfert C, Sundberg C, Sevigny J, Enjyoji K, Hoshi T, Csizmadia E, and Robson S (2001). Disordered cellular migration and angiogenesis in CD39-null mice. *Circulation* **104**, 3109–3115.

[38] White N, Knight GE, Butler PE, and Burnstock G (2009). An *in vivo* model of melanoma: treatment with ATP. *Purinergic Signal* **5**, 327–333.

[39] Humphreys BD, Virginio C, Surprenant A, Rice J, and Dubyak GR (1998). Isoquinolines as antagonists of the P2X7 nucleotide receptor: high selectivity for the human *versus* rat receptor homologues. *Mol Pharmacol* **54**, 22–32.

[40] Fang WG, Pirnia F, Bang YJ, Myers CE, and Trepel JB (1992). P2-purinergic receptor agonists inhibit the growth of androgen-independent prostate carcinoma cells. *J Clin Invest* **89**, 191–196.

[41] Zhou Q, Yan J, Putheti P, Wu Y, Sun X, Toxavidis V, Tigges J, Kassam N, Enjyoji K, Robson SC, et al. (2009). Isolated CD39 expression on $CD4^+$ T cells denotes both regulatory and memory populations. *Am J Transplant* **9**, 2303–2311.

[42] Goepfert C, Imai M, Brouard S, Csizmadia E, Kaczmarek E, and Robson SC (2000). CD39 modulates endothelial cell activation and apoptosis. *Mol Med* **6**, 591–603.

[43] Merighi S, Mirandola P, Milani D, Varani K, Gessi S, Klotz KN, Leung E, Baraldi PG, and Borea PA (2002). Adenosine receptors as mediators of both

cell proliferation and cell death of cultured human melanoma cells. *J Invest Dermatol* **119**, 923–933.

[44] Merighi S, Mirandola P, Varani K, Gessi S, Leung E, Baraldi PG, Tabrizi MA, and Borea PA (2003). A glance at adenosine receptors: novel target for antitumor therapy. *Pharmacol Ther* **100**, 31–48.

[45] Panjehpour M and Karami-Tehrani F (2007). Adenosine modulates cell growth in the human breast cancer cells via adenosine receptors. *Oncol Res* **16**, 575–585.

[46] Kim SJ, Min HY, Chung HJ, Park EJ, Hong JY, Kang YJ, Shin DH, Jeong LS, and Lee SK (2008). Inhibition of cell proliferation through cell cycle arrest and apoptosis by thio-Cl-IB-MECA, a novel A3 adenosine receptor agonist, in human lung cancer cells. *Cancer Lett* **264**, 309–315.

[47] Fishman P, Bar-Yehuda S, Madi L, and Cohn I (2002). A3 adenosine receptor as a target for cancer therapy. *Anticancer Drugs* **13**, 437–443.

[48] Fishman P, Bar-Yehuda S, Ohana G, Barer F, Ochaion A, Erlanger A, and Madi L (2004). An agonist to the A3 adenosine receptor inhibits colon carcinoma growth in mice via modulation of GSK-3 β and NF-κB. *Oncogene* **23**, 2465–2471.

[49] Dzhandzhugazyan KN, Kirkin AF, thor Straten P, and Zeuthen J (1998). Ecto-ATP diphosphohydrolase/CD39 is overexpressed in differentiated human melanomas. *FEBS Lett* **430**, 227–230.

[50] Jin D, Fan J, Wang L, Thompson LF, Liu A, Daniel BJ, Shin T, Curiel TJ, and Zhang B (2010). CD73 on tumor cells impairs antitumor T-cell responses: a novel mechanism of tumor-induced immune suppression. *Cancer Res* **70**, 2245–2255.